EUROPEAN ORGANIZATION FOR NUCLEAR RESEARCH

CERN-PPE/97-67
13 June 1997

Measurement of W-Pair Cross Sections in e^+e^- Interactions at $\sqrt{s} = 172$ GeV and W-Decay Branching Fractions

The L3 Collaboration

Abstract

We report on the measurement of W-boson pair-production with the L3 detector at LEP at an average centre-of-mass energy of 172.13 GeV. In a data sample corresponding to a total luminosity of 10.25 pb^{-1} we select 110 four-fermion events with pairs of hadronic jets or leptons with high invariant masses. Branching fractions of W decays into different fermion-antifermion pairs are determined with and without the assumption of charged-current lepton universality. The branching fraction for hadronic W decays is measured to be: $B(\mathrm{W} \to \mathrm{hadrons}) = 64.2^{+3.7}_{-3.8}$ (*stat.*) $\pm$ 0.5 (*syst.*) %. Combining all final states the total cross section for W-pair production is measured to be: $\sigma_{\mathrm{WW}} = 12.27^{+1.41}_{-1.32}$ (*stat.*) $\pm$ 0.23 (*syst.*) pb. The results are in good agreement with the Standard Model.

Submitted to *Phys. Lett. B*

1 Introduction

In the second half of the 1996 data taking period, the e^+e^- collider LEP at CERN was operated at centre-of-mass energies, $\sqrt{s}$, above the kinematic threshold of W-pair production, $e^+e^- \to W^+W^-$, which was investigated earlier at LEP [1, 2]. Compared to the situation at threshold the higher centre-of-mass energy implies an increased cross section for the W-pair signal and a reduced cross section for the fermion-pair background, thus improving the signal-to-background ratio by a factor of four.

To lowest order within the Standard Model [3], three Feynman diagrams contribute to W-pair production, the s-channel γ and Z-boson exchange and the t-channel ν_e exchange, referred to as CC03 [4–6]. The higher centre-of-mass energy increases the importance of the s-channel diagrams. The W boson decays into a quark-antiquark pair, for example $W^- \to \bar{u}d$ or $\bar{c}s$, or a lepton-antilepton pair, $W^- \to \ell^-\bar{\nu}_\ell$ ($\ell = e, \mu, \tau$); in the following denoted as qq, $\ell\nu$ or ff in general for both W^+ and W^- decays. In this letter, separate measurements of all four-fermion final states mediated by W-pair production are reported:

1. $e^+e^- \to qqe\nu(\gamma)$ 2. $e^+e^- \to qq\mu\nu(\gamma)$ 3. $e^+e^- \to qq\tau\nu(\gamma)$

4. $e^+e^- \to \ell\nu\ell\nu(\gamma)$ 5. $e^+e^- \to qqqq(\gamma)$,

where (γ) indicates the possible presence of radiative photons. Additional contributions to the production of these four-fermion final states arising from other neutral-current (NC) or charged-current (CC) Feynman diagrams are small. At the current level of statistical accuracy the interference effects need to be taken into account only for $e^+e^- \to qqe\nu(\gamma)$ (CC20) and $e^+e^- \to \ell\nu\ell\nu(\gamma)$ (CC56+NC56) [4–6].

During the run the L3 detector collected integrated luminosities of 1.00 pb^{-1} and 9.25 pb^{-1} at $\sqrt{s} = 170.31 \pm 0.06$ GeV and $\sqrt{s} = 172.32 \pm 0.06$ GeV, respectively [7]. For the results presented here these two data samples are combined using a luminosity weighted mean centre-of-mass energy of $\sqrt{s} = 172.13 \pm 0.06$ GeV. The cross section is measured for each of the five signal processes. Combining these measurements the W-decay branching fractions and the total W-pair production cross section are determined.

2 Analysis of Four-Fermion Production

The L3 detector is described in detail in References 8 and 9. The selections of the five four-fermion final states are similar to the ones used at $\sqrt{s} = 161$ GeV [1]. Charged leptons are explicitly identified using their characteristic signature. Hadronic jets are reconstructed using the Durham jet algorithm [10] and adding four-momenta during the combination process. The momentum of the neutrino in $qq\ell\nu$ events is identified with the missing momentum vector.

Selection efficiencies and background contaminations of all processes are determined by Monte Carlo simulations. The following Monte Carlo event generators are used to simulate the various signal and background reactions: KORALW [11] and HERWIG [12] ($e^+e^- \to WW \to ffff(\gamma)$); EXCALIBUR [13] ($e^+e^- \to ffff(\gamma)$); PYTHIA [14] ($e^+e^- \to q\bar{q}(\gamma), ZZ(\gamma)$, hadronic two-photon collisions); KORALZ [15] ($e^+e^- \to \mu^+\mu^-(\gamma),\ \tau^+\tau^-(\gamma)$); BHAGENE3 [16] ($e^+e^- \to e^+e^-(\gamma)$). The response of the L3 detector is modelled with the GEANT [17] detector simulation program which includes the effects of energy loss, multiple scattering and showering in the detector materials and in the beam pipe.

Systematic errors on the cross-section measurements are in all cases small compared to the

statistical error. The measurement of the total luminosity, $\mathcal{L}$, follows the procedure described in References 18 and 19. The total error on the luminosity measurement is estimated to be 0.6% [19].

The results on cross sections and W-decay branching fractions are determined in a combined fit as discussed in Section 3. They are compared to the predictions of the Standard Model calculated for a mass of the W boson of $M_W = 80.33$ GeV [20] using the GENTLE [21] program.

2.1 $e^+e^- \to qqe\nu(\gamma)$

There are several changes in the event selection for the process $e^+e^- \to qqe\nu(\gamma)$ at $\sqrt{s} = 172$ GeV relative to that at $\sqrt{s} = 161$ GeV [1]. The neutrino energy must be larger than 20 GeV and the range of accepted polar angles of electron and neutrino, θ_e and θ_ν, is extended to $|\cos\theta_e|, |\cos\theta_\nu| < 0.95$. The electron identification in the forward-backward region, $|\cos\theta_e| > 0.75$, is improved by widening the window in azimuthal angle, $|\Delta\phi|$, for associating a track in the central tracking chamber to the calorimetric energy deposition. Depending on $|\cos\theta_e|$, the $|\Delta\phi|$ window is enlarged from 10 mrad up to 42 mrad to account for geometrical and resolution effects.

After having removed the calorimetric energy depositions associated with the identified electron, the remaining calorimetric clusters are grouped into two jets. To reject electrons from decays of hadrons the separation angle between the electron and both hadronic jets must be larger than ten degrees. The invariant masses of the electron-neutrino system, $M_{e\nu}$, and the jet-jet system, M_{qq}, are required to be larger than 55 GeV and 45 GeV, respectively.

The distributions of the polar angle of the neutrino and of the invariant mass of the electron-neutrino system are shown in Figure 1, comparing Monte Carlo to data.

A total of 19 events are selected in the data. The selection efficiencies and the background contributions are listed in Table 1. The signal efficiency and cross section is determined within the following phase-space cuts: $E_e, E_\nu > 20$ GeV; $|\cos\theta_e|, |\cos\theta_\nu| < 0.95$; $M_{e\nu}, M_{qq} > 45$ GeV.

Systematic errors in the electron identification are derived from a comparison of data versus Monte Carlo using $e^+e^- \to e^+e^-(\gamma)$ events collected at $\sqrt{s} = 91$ GeV and radiative $e^+e^- \to q\bar{q}(\gamma)$ events as control samples. Systematic errors on efficiencies and accepted background cross sections are derived by comparing different Monte Carlo event generators and Monte Carlo samples simulated with different W masses and detector energy scales. A total systematic error of 3% on the measured cross section is obtained.

2.2 $e^+e^- \to qq\mu\nu(\gamma)$

The event selection for the process $e^+e^- \to qq\mu\nu(\gamma)$ is adapted to the higher centre-of-mass energy. The selection is improved by including muons identified by their minimum-ionising-particle (MIP) signature in the calorimeters. If two muons are reconstructed the invariant mass of the two-muon system must be smaller than 30 GeV. After having removed the calorimetric energy depositions associated with the identified muon, the remaining calorimetric clusters are grouped into two jets.

Muons identified in the muon spectrometer must have a momentum larger than 15 GeV. Their angular separation to both hadronic jets must be at least ten degrees to reject muons arising from the decays of hadrons. The muon-neutrino invariant mass must be larger than 55 GeV, and the jet-jet invariant mass must be larger than 30 GeV and smaller than 120 GeV.

Muons are also identified as a track in the central tracking chamber with momentum larger than 10 GeV associated with energy depositions in the calorimeters compatible with those of a MIP. Muons identified as MIPs in the electromagnetic and hadronic calorimeters must have an angular separation of at least 15 degrees to both hadronic jets while muons identified in the electromagnetic calorimeter only must have at least 20 degrees angular separation. For MIP muons the muon-neutrino invariant mass must be larger than 20 GeV, and the jet-jet invariant mass must be larger than 40 GeV and smaller than 110 GeV. The inclusion of MIP-based muon identification increases the selection efficiency by 10%.

The distributions of the polar angle of the neutrino and of the invariant mass of the muon-neutrino system are shown in Figure 2.

A total of nine events are selected in the data, eight events with a muon reconstructed in the muon spectrometer and one event with a muon identified by its MIP signature. The selection efficiencies and the background contributions are listed in Table 1.

Systematic errors in the muon and MIP identification are derived from a comparison of data versus Monte Carlo using $e^+e^- \to \mu^+\mu^-(\gamma)$ and $e^+e^- \to q\bar{q}(\gamma)$ events collected at $\sqrt{s} = 91$ GeV as a control sample. Systematic errors on efficiencies and accepted background cross sections are evaluated as described at the end of Section 2.1. A total systematic error of 3% on the measured cross section is obtained.

2.3 $e^+e^- \to q\bar{q}\tau\nu(\gamma)$

Events must have more than 15 calorimetric clusters in order to reject low-multiplicity leptonic final states. Signal events contain at least two neutrinos, resulting in missing momentum and reduced visible energy. In order to reject $q\bar{q}(\gamma)$ and $qqqq(\gamma)$ events the missing momentum must be larger than 10 GeV, while the difference between the visible energy and the missing momentum must be less than 130 GeV. Requiring the longitudinal energy imbalance to be smaller than 40 GeV and the transverse energy imbalance to be larger than 5 GeV suppresses $q\bar{q}(\gamma)$ events with hard initial-state radiation.

In events with the τ decaying into an electron or muon, the energy of that lepton must be larger than 5 GeV and the sum of the electron (muon) energy and the magnitude of the missing momentum must be less than 70 GeV (65 GeV).

If no electrons or muons are found, jets are reconstructed based on clustering inside a cone of 15 degrees half-opening angle [22]. At least three jets with an energy larger than 10 GeV are required. The hadronically decaying τ is identified among the three jets of highest energy as the one which satisfies the largest number of the following requirements for being τ-like: the number of tracks associated to the jet is between one and three, the number of calorimetric clusters associated to the jet is less than five, the half-opening angle of the jet is less than eight degrees, the electromagnetic energy of the jet is greater than 25 GeV, and the visible mass of the jet is less than 2 GeV. The efficiency of this τ jet identification for hadronic τ decays is 80%. In order to reduce the background from $e^+e^- \to qqe\nu(\gamma)$ events where the electron is not identified, events with the τ jet having more than 30 GeV of energy deposited in the electromagnetic calorimeter and less than 5 GeV in the hadronic calorimeter are rejected. The background of $e^+e^- \to qq\mu\nu(\gamma)$ events where the muon is not identified in the muon chambers is reduced by rejecting events where the τ jet is compatible with a MIP.

After having removed the tracks and calorimetric energy depositions associated with the identified τ jet, the remaining tracks and calorimetric clusters are grouped into two hadronic jets using the Durham jet algorithm [10]. For events with a transverse energy imbalance less

than 25 GeV and with $|\cos\theta_{miss}| > 0.55$ for the polar angle of the missing momentum vector, the angular opening of the τ jet must be smaller than eight degrees. The invariant mass of the jet-jet system must be larger than 60 GeV and smaller than 100 GeV. The system of the τ jet and the missing four-momentum must have an invariant mass larger than 50 GeV and smaller than 110 GeV.

The distributions of the sum of the electron (muon) energy and the missing momentum, and of the invariant mass of the system of the τ jet and the missing four-momentum are shown in Figure 3.

A total of twelve events are selected in the data, two $\tau \to$ e events, three $\tau \to \mu$ events and seven $\tau \to$hadrons events. The selection efficiencies and the background contributions are listed in Table 1. Systematic errors are evaluated as described at the end of Sections 2.1 and 2.2. A total systematic error of 5% on the measured cross section is obtained.

2.4 $e^+e^- \to \ell\nu\ell\nu(\gamma)$

The event selection for the process $e^+e^- \to \ell\nu\ell\nu(\gamma)$ depends on whether the event contains one or two identified electrons or muons, referred to as lepton-jet and lepton-lepton class. The selection for the lepton-jet class is the same as at $\sqrt{s} = 161$ GeV [1]. For the lepton-lepton class, the transverse energy must be at least 10 GeV and larger than 10% of the visible energy. The requirement of the missing energy vector not pointing to the gap between the electromagnetic barrel and endcap calorimeter is no longer necessary because of the use of a new electromagnetic calorimeter in that region [9]. The sum of the energies of calorimetric clusters at low polar angles, $|\cos\theta_{cluster}| > 0.95$, must be less than 5 GeV.

The distributions of the acoplanarity between the two charged leptons and of the energy of the identified electron or muon with highest energy are shown in Figure 4.

A total of nine events are selected in the data, five events in the lepton-lepton class and four events in the lepton-jet class. The selection efficiencies and the background contributions are listed in Table 1. The signal efficiency and cross section is determined within the following phase-space cuts: $|\cos\theta| < 0.96$ for both charged leptons, with energies larger than 15 GeV and 5 GeV.

Systematic errors on the lepton identification are derived from a comparison of data versus Monte Carlo using $e^+e^- \to \ell^+\ell^-(\gamma)$ events as a control sample. Systematic errors on efficiencies and accepted background cross sections are evaluated as described at the end of Section 2.1. A total systematic error of 4% on the measured cross section is obtained.

2.5 $e^+e^- \to qqqq(\gamma)$

The event selection for the process $e^+e^- \to qqqq(\gamma)$ is similar to that at $\sqrt{s} = 161$ GeV [1]. High multiplicity events with visible energy, $E_{\rm vis}$, larger than $0.7\sqrt{s}$ and longitudinal energy imbalance less than $0.25E_{\rm vis}$ are selected. Tracks and calorimetric clusters are grouped into four jets. The Durham jet-resolution parameter [10] at which the event changes from a four-jet to a three-jet topology, Y_{34}, must be larger than 0.0025 to enhance the four-jet signal. To suppress $q\bar{q}(\gamma)$ background with hard radiative photons recorded in the detector, an event is rejected if it contains an electromagnetic cluster with an energy of more than 40 GeV, or if more than 50% of energy of any jet is attributed to a single photon.

The selection accepts 92.3% of the WW $\to qqqq(\gamma)$ signal while reducing the dominating $q\bar{q}(\gamma)$ background by a factor of 20. A total of 122 events pass this selection. The determination

of jet energies and angles is improved by a kinematic fit imposing four-momentum conservation. Two pairs of jets are formed with invariant masses M_1 and M_2. The optimal jet-jet pairing maximising the sum $M_1 + M_2 + \min(M_1, M_2)$ is chosen. This yields the correct assignment of jets to W bosons for 76% of the selected signal events.

A neural network is trained to separate the signal from the dominating $q\bar{q}(\gamma)$ background. The input to the network consists of ten variables: Y_{34}, sphericity, minimal and maximal jet energies, minimal jet cluster multiplicity, sum and difference of the two W masses, maximal acollinearity between jets belonging to the same W, minimal jet-jet angle, minimal mass of jets when the event is reconstructed as a two-jet event. The network is trained such that the output peaks at one for the signal and at zero for the background.

The distributions of the jet resolution parameter Y_{34}, the minimal jet-jet angle and the minimal and maximal jet energies are shown in Figure 5. In projection, these four neural-network input variables show the largest separation between the signal and the background. The distribution of the neural-network output is shown in Figure 6.

The neural-network output distribution for data events is fitted by a linear combination of neural-network output distributions derived from Monte Carlo simulations for signal and background [1]. The results of the fit correspond to a signal cross section of $5.48^{+0.92}_{-0.85}$ pb and a $q\bar{q}(\gamma)$ cross section of 128^{+18}_{-17} pb where the errors are statistical. The measured $q\bar{q}(\gamma)$ cross section is in good agreement with both our dedicated measurements of fermion-pair cross sections [19] and with the Standard Model value. As a cross check the signal cross section is determined by applying a cut on the output of the neural network larger than 0.72. The selection efficiencies and the background contributions corresponding to this cut are listed in Table 1. A total of 61 events are selected in the data, yielding a signal cross section of $5.57^{+0.95}_{-0.87}$ pb.

The systematic error due to a discrepancy in the four-jet event rate between the $q\bar{q}(\gamma)$ data and the Monte Carlo is estimated to be 2% by reweighting $q\bar{q}(\gamma)$ Monte Carlo events as a function of Y_{34}. The reweighting function is derived from a comparison between data and Monte Carlo of hadronic Z decays collected at $\sqrt{s} = 91$ GeV. Systematic effects due to Bose-Einstein correlations and fragmentation models are estimated to be 2% by comparing different Monte Carlo programs to simulate the signal. Detector calibration uncertainties and W-mass dependence lead to an error of less than 2%. A total systematic error of 3% on the measured cross section is obtained.

3 Results

The fitting procedure to determine cross sections of the five signal processes, W-decay branching fractions, the total W-pair cross section and the mass of the W boson is described in detail in Reference 1.

3.1 Signal Cross Sections

The cross sections, σ_i, of the five signal processes are determined simultaneously in a maximum-likelihood fit, using the number of selected events, selection efficiencies and accepted background cross sections as summarised in Tables 1 and 2. For the $e^+e^- \to qqq(\gamma)$ process, the likelihood as a function of the signal cross section derived from the fit to the neural-network output distribution described in Section 2.5 is used.

The resulting cross sections including statistical and systematic errors are listed in Table 2. The Standard Model agrees well with these results. Since the efficiency matrix of Table 1

contains non-zero off-diagonal elements, the measured cross sections are correlated. The largest correlations, -13% and -17%, arise among the semileptonic channels between $qq\tau\nu$ and $qqe\nu$ and between $qq\tau\nu$ and $qq\mu\nu$. All other correlations are smaller than 1% in magnitude and thus negligible.

For the $qqe\nu(\gamma)$ and $\ell\nu\ell\nu(\gamma)$ final state the cross sections contain significant contributions from processes not mediated by resonant W-pair production. In order to determine W-pair cross sections also for these final states the measured cross sections are scaled by a multiplicative factor, f_i. These conversion factors are given by the ratio of the total CC03 cross section and the four-fermion cross section within phase-space cuts, and are calculated within the Standard Model using the EXCALIBUR [13] event generator. They are determined to be 1.10 for the $qqe\nu(\gamma)$ and 1.03 for the $\ell\nu\ell\nu(\gamma)$ phase-space cuts, where the dependence of the f_i on $\mathrm{M_W}$ is negligible. These cross sections are also listed in Table 2.

3.2 W-Decay Branching Fractions and W-Pair Cross Section

For the determination of the total CC03 production cross section of W-pairs, σ_{WW}, the signal cross sections σ_i are replaced by the product $r_i\sigma_{\mathrm{WW}}$ or $r_i\sigma_{\mathrm{WW}}/f_i$ for the $qqe\nu(\gamma)$ and $\ell\nu\ell\nu(\gamma)$ final states. The ratios r_i are given in terms of the W-decay branching fractions, $B(\mathrm{W}\to qq)$ and $B(\mathrm{W}\to\ell\nu)$, as follows: $r_{qqqq}=[B(\mathrm{W}\to qq)]^2$, $r_{qq\ell\nu}=2B(\mathrm{W}\to qq)B(\mathrm{W}\to\ell\nu)$, and $r_{\ell\nu\ell\nu}=[1-B(\mathrm{W}\to qq)]^2$, where the sum of the hadronic and the three leptonic branching fractions is constrained to be unity. For the determination of W-decay branching fractions the data collected at $\sqrt{s}=161$ GeV [1] are included.

The resulting total W-pair cross section and the W-decay branching fractions including statistical and systematic errors are listed in Table 3. They are determined both with and without the assumption of charged-current lepton universality in W decays. The W-decay branching fractions obtained for the individual leptons are in agreement with each other and support this assumption. The branching fraction for hadronic W decays is:

$$B(\mathrm{W}\to\mathrm{qq}) \;=\; 64.2^{+3.7}_{-3.8}\;(stat.)\pm 0.5\;(syst.)\;\%\,. \qquad (1)$$

The accuracy on the W-decay branching fractions is improved by more than a factor of two with respect to our previous analysis [1].

Within the Standard Model the branching fractions of the W boson depend on the six elements V_{qq} of the Cabibbo-Kobayashi-Maskawa quark mixing matrix V_{CKM} [23] not involving the top quark. In terms of these V_{qq} the branching fraction of leptonic W decays is given by $1/B(\mathrm{W}\to\ell\nu)=3+3[1+\alpha_{\mathrm{s}}(\mathrm{M_W})/\pi]\sum|V_{qq}|^2$, where α_{s} is the strong coupling constant [5]. The sensitivity is largest for the dominant diagonal elements of V_{CKM}. Since V_{ud} is known much more precisely than V_{cs}, it is most useful to determine the latter. Using the current world-average values and errors of the other matrix elements not assuming the unitarity of V_{CKM} [24], the result is:

$$|V_{\mathrm{cs}}| \;=\; 0.82^{+0.17}_{-0.18}\;(stat.)\pm 0.02\;(syst.)\,. \qquad (2)$$

The statistical error includes the errors on α_{s} and the other V_{qq} but is dominated by the statistical error on the W branching fractions. This result is of the same precision as the current world average [24].

In order to obtain a more precise determination of σ_{WW}, the W-decay branching fractions from the Standard Model are imposed, which are calculated including QCD and mass

corrections [5] (Table 3). The result for the total production cross section of W-pairs at $\sqrt{s} = 172.13 \pm 0.06$ GeV [7] is:

$$\sigma_{\mathrm{WW}} \;=\; 12.27^{+1.41}_{-1.32}\;(stat.) \pm 0.23\;(syst.)\;\mathrm{pb}\,. \tag{3}$$

The measurements of σ_{WW} at $\sqrt{s} = 161$ GeV [1] and at $\sqrt{s} = 172$ GeV are compared to the Standard Model expectations in Figure 7. The deviation to pure t-channel ν_{e} exchange in W-pair production is clearly visible. Both non-abelian s-channel diagrams with triple-vector-boson couplings as expected within the Standard Model are needed to get agreement with the measurement presented here.

Within the Standard Model the W-pair cross section, σ_{WW}, depends on $\sqrt{s}$ and the mass of the W boson, $\mathrm{M_W}$. The sensitivity of σ_{WW} to $\mathrm{M_W}$ at $\sqrt{s} = 172$ GeV is reduced compared to that at $\sqrt{s} = 161$ GeV [25]. The cross section measurement presented here yields $\mathrm{M_W} = 80.5^{+1.4}_{-2.4}\;(stat.) \pm 0.3\;(syst.)$ GeV. Combining this new measurement with our previous result on $\mathrm{M_W}$ obtained from the cross section measurement at $\sqrt{s} = 161$ GeV [1] one finds $\mathrm{M_W} = 80.78^{+0.45}_{-0.41}\;(exp.) \pm 0.03$ (LEP) GeV. These results for $\mathrm{M_W}$ are based on total cross section measurements only. The mass of the W boson as determined more precisely from the invariant mass of the W decay products will be presented in a forthcoming publication [26].

4 Acknowledgements

We wish to congratulate the CERN accelerator divisions for the successful upgrade of the LEP machine and to express our gratitude for its good performance. We acknowledge with appreciation the effort of all engineers, technicians and support staff who have participated in the construction and maintenance of this experiment.

References

[1] The L3 Collaboration, M. Acciarri *et al.*, Phys. Lett. **B 398** (1997) 223.

[2] The ALEPH Collaboration, R. Barate *et al.*, Phys. Lett. **B 401** (1997) 347;
The DELPHI Collaboration, P. Abreu *et al.*, Phys. Lett. **B 397** (1997) 158;
The OPAL Collaboration, K. Ackerstaff *et al.*, Phys. Lett. **B 389** (1996) 416; Phys. Lett. **B 397** (1997) 147.

[3] S. L. Glashow, Nucl. Phys. **22** (1961) 579;
S. Weinberg, Phys. Rev. Lett. **19** (1967) 1264;
A. Salam, in *Elementary Particle Theory*, ed. N. Svartholm, Stockholm, Almquist and Wiksell (1968), 367.

[4] D. Bardin *et al.*, Nucl. Phys. (Proc. Suppl.) **B 37** (1994) 148;
F.A. Berends *et al.*, Nucl. Phys. (Proc. Suppl.) **B 37** (1994) 163.

[5] W. Beenakker *et al.*, in *Physics at LEP 2*, Report CERN 96-01 (1996), eds G. Altarelli, T. Sjöstrand, F. Zwirner, Vol. 1, p. 79.

[6] D. Bardin *et al.*, in *Physics at LEP 2*, Report CERN 96-01 (1996), eds G. Altarelli, T. Sjöstrand, F. Zwirner, Vol. 2, p. 3.

[7] The working group on LEP energy, *LEP Energy Calibration in 1996*, LEP Energy Group/97-01.

[8] The L3 Collaboration, B. Adeva *et al.*, Nucl. Instr. and Meth. **A 289** (1990) 35;
M. Chemarin *et al.*, Nucl. Instr. and Meth. **A 349** (1994) 345;
M. Acciarri *et al.*, Nucl. Instr. and Meth. **A 351** (1994) 300;
I.C. Brock *et al.*, Nucl. Instr. and Meth. **A 381** (1996) 236;
A. Adam *et al.*, Nucl. Instr. and Meth. **A 383** (1996) 342.

[9] G. Basti *et al.*, Nucl. Instr. and Meth. **A 374** (1996) 293.

[10] S. Catani *et al.*, Phys. Lett. **B 269** (1991) 432;
S. Bethke *et al.*, Nucl. Phys. **B 370** (1992) 310.

[11] The KORALW version 1.21 is used.
M. Skrzypek, S. Jadach, W. Placzek and Z. Wąs, Comp. Phys. Comm. **94** (1996) 216;
M. Skrzypek, S. Jadach, M. Martinez, W. Placzek and Z. Wąs, Phys. Lett. **B 372** (1996) 289.

[12] The HERWIG version 5.9 is used.
G. Marchesini and B. Webber, Nucl. Phys. **B 310** (1988) 461;
I.G. Knowles, Nucl. Phys. **B 310** (1988) 571;
G. Marchesini *et al.*, Comp. Phys. Comm. **67** (1992) 465.

[13] F.A. Berends, R. Kleiss and R. Pittau, Nucl. Phys. **B 424** (1994) 308; Nucl. Phys. **B 426** (1994) 344; Nucl. Phys. (Proc. Suppl.) **B 37** (1994) 163;
R. Kleiss and R. Pittau, Comp. Phys. Comm. **83** (1994) 141;
R. Pittau, Phys. Lett. **B 335** (1994) 490.

[14] T. Sjöstrand, *PYTHIA 5.7 and JETSET 7.4 Physics and Manual*, CERN-TH/7112/93 (1993), revised August 1995; Comp. Phys. Comm. **82** (1994) 74.

[15] The KORALZ version 4.01 is used.
S. Jadach, B. F. L. Ward and Z. Wąs, Comp. Phys. Comm. **79** (1994) 503.

[16] J.H. Field, Phys. Lett. **B 323** (1994) 432;
J.H. Field and T. Riemann, Comp. Phys. Comm. **94** (1996) 53.

[17] The L3 detector simulation is based on GEANT Version 3.15.
R. Brun *et al.*, *GEANT 3*, CERN-DD/EE/84-1 (Revised), 1987.
The GHEISHA program (H. Fesefeldt, RWTH Aachen Report PITHA 85/02 (1985)) is used to simulate hadronic interactions.

[18] The L3 Collaboration, M. Acciarri *et al.*, Z. Phys. **C 62** (1994) 551.

[19] The L3 Collaboration, M. Acciarri *et al.*, *Measurement of Hadron and Lepton-Pair Production at 161 GeV* $< \sqrt{s} <$ *172 GeV at LEP*, CERN-PPE/97-52.

[20] The UA1 Collaboration, C. Albajar *et al.*, Z. Phys. **C 44** (1989) 15;
The UA2 Collaboration, J. Alitti *et al.*, Phys. Lett. **B 241** (1990) 150; Phys. Lett. **B 276** (1992) 354;
The CDF Collaboration, F. Abe *et al.*, Phys. Rev. Lett. **65** (1990) 2243; Phys. Rev. **D 43** (1991) 2070; Phys. Rev. Lett. **75** (1995) 11; Phys. Rev. **D 52** (1995) 4784;
The DØ Collaboration, S. Abachi *et al.*, Phys. Rev. Lett. **77** (1996) 3309.
We use the average value and error for the mass of the W boson as listed in:
R.M. Barnett *et al.*, *Review of Particle Properties*, Phys. Rev. **D 54** (1996) 1.

[21] The GENTLE version 2.0 is used.
D. Bardin *et al.*, *GENTLE/4fan v. 2.0: A Program for the Semi-Analytic Calculation of Predictions for the Process* $e^+e^- \to 4f$, DESY 96-233, hep-ph/9612409.

[22] H.J. Daum *et al.*, Z. Phys. **C 8** (1981) 167.

[23] N. Cabibbo, Phys. Rev. Lett. **10** (1963) 531;
M. Kobayashi and T. Maskawa, Prog. Theor. Phys. **49** (1973) 652.

[24] R.M. Barnett *et al.*, *Review of Particle Properties*, Phys. Rev. **D 54** (1996) 94;
and references therein.

[25] Z. Kunszt *et al.*, in *Physics at LEP 2*, Report CERN 96-01 (1996), eds G. Altarelli, T. Sjöstrand, F. Zwirner, Vol. 1, p. 141.

[26] The L3 Collaboration, M. Acciarri *et al.*, in preparation.

The L3 Collaboration:

M.Acciarri,[29] O.Adriani,[18] M.Aguilar-Benitez,[28] S.Ahlen,[12] J.Alcaraz,[28] G.Alemanni,[24] J.Allaby,[19] A.Aloisio,[31] G.Alverson,[13] M.G.Alviggi,[31] G.Ambrosi,[21] H.Anderhub,[51] V.P.Andreev,[7,40] T.Angelescu,[14] F.Anselmo,[10] A.Arefiev,[30] T.Azemoon,[3] T.Aziz,[11] P.Bagnaia,[39] L.Baksay,[46] S.Banerjee,[11] Sw.Banerjee,[11] K.Banicz,[48] A.Barczyk,[51,49] R.Barillère,[19] L.Barone,[39] P.Bartalini,[36] A.Baschirotto,[29] M.Basile,[10] R.Battiston,[36] A.Bay,[24] F.Becattini,[18] U.Becker,[17] F.Behner,[51] J.Berdugo,[28] P.Berges,[17] B.Bertucci,[36] B.L.Betev,[51] S.Bhattacharya,[11] M.Biasini,[19] A.Biland,[51] G.M.Bilei,[36] J.J.Blaising,[4] S.C.Blyth,[37] G.J.Bobbink,[2] R.Bock,[1] A.Böhm,[1] L.Boldizsar,[15] B.Borgia,[39] D.Bourilkov,[51] M.Bourquin,[21] S.Braccini,[21] J.G.Branson,[42] V.Brigljevic,[51] I.C.Brock,[37] A.Buffini,[18] A.Buijs,[47] J.D.Burger,[17] W.J.Burger,[21] J.Busenitz,[46] A.Button,[3] X.D.Cai,[17] M.Campanelli,[51] M.Capell,[17] G.Cara Romeo,[10] G.Carlino,[31] A.M.Cartacci,[18] J.Casaus,[28] G.Castellini,[18] F.Cavallari,[39] N.Cavallo,[31] C.Cecchi,[21] M.Cerrada,[28] F.Cesaroni,[25] M.Chamizo,[28] Y.H.Chang,[53] U.K.Chaturvedi,[20] S.V.Chekanov,[33] M.Chemarin,[27] A.Chen,[53] G.Chen,[8] G.M.Chen,[8] H.F.Chen,[22] H.S.Chen,[8] X.Chereau,[4] G.Chiefari,[31] C.Y.Chien,[5] L.Cifarelli,[41] F.Cindolo,[10] C.Civinini,[18] I.Clare,[17] R.Clare,[17] H.O.Cohn,[34] G.Coignet,[4] A.P.Colijn,[2] N.Colino,[28] V.Commichau,[1] S.Costantini,[9] F.Cotorobai,[14] B.de la Cruz,[28] A.Csilling,[15] T.S.Dai,[17] R.D'Alessandro,[18] R.de Asmundis,[31] A.Degré,[4] K.Deiters,[49] D.della Volpe,[31] P.Denes,[38] F.DeNotaristefani,[39] D.DiBitonto,[46] M.Diemoz,[39] D.van Dierendonck,[2] F.Di Lodovico,[51] C.Dionisi,[39] M.Dittmar,[51] A.Dominguez,[42] A.Doria,[31] M.T.Dova,[20,♯] D.Duchesneau,[4] P.Duinker,[2] I.Duran,[43] S.Dutta,[11] S.Easo,[36] Yu.Efremenko,[34] H.El Mamouni,[27] A.Engler,[37] F.J.Eppling,[17] F.C.Erné,[2] J.P.Ernenwein,[27] P.Extermann,[21] M.Fabre,[49] R.Faccini,[39] S.Falciano,[39] A.Favara,[18] J.Fay,[27] O.Fedin,[40] M.Felcini,[51] B.Fenyi,[46] T.Ferguson,[37] F.Ferroni,[39] H.Fesefeldt,[1] E.Fiandrini,[36] J.H.Field,[21] F.Filthaut,[37] P.H.Fisher,[17] I.Fisk,[42] G.Forconi,[17] L.Fredj,[21] K.Freudenreich,[51] C.Furetta,[29] Yu.Galaktionov,[30,17] S.N.Ganguli,[11] P.Garcia-Abia,[50] S.S.Gau,[13] S.Gentile,[39] N.Gheordanescu,[14] S.Giagu,[39] S.Goldfarb,[24] J.Goldstein,[12] Z.F.Gong,[22] A.Gougas,[5] G.Gratta,[35] M.W.Gruenewald,[9] V.K.Gupta,[38] A.Gurtu,[11] L.J.Gutay,[48] B.Hartmann,[1] A.Hasan,[32] D.Hatzifotiadou,[10] T.Hebbeker,[9] A.Hervé,[19] W.C.van Hoek,[33] H.Hofer,[51] S.J.Hong,[45] H.Hoorani,[37] S.R.Hou,[53] G.Hu,[5] V.Innocente,[19] K.Jenkes,[1] B.N.Jin,[8] L.W.Jones,[3] P.de Jong,[19] I.Josa-Mutuberria,[28] A.Kasser,[24] R.A.Khan,[20] D.Kamrad,[50] Yu.Kamyshkov,[34] J.S.Kapustinsky,[26] Y.Karyotakis,[4] M.Kaur,[20,◇] M.N.Kienzle-Focacci,[21] D.Kim,[39] D.H.Kim,[45] J.K.Kim,[45] S.C.Kim,[45] Y.G.Kim,[45] W.W.Kinnison,[26] A.Kirkby,[35] D.Kirkby,[35] J.Kirkby,[19] D.Kiss,[15] W.Kittel,[33] A.Klimentov,[17,30] A.C.König,[33] A.Kopp,[50] I.Korolko,[30] V.Koutsenko,[17,30] R.W.Kraemer,[37] W.Krenz,[1] A.Kunin,[17,30] P.Ladron de Guevara,[28] I.Laktineh,[27] G.Landi,[18] C.Lapoint,[17] K.Lassila-Perini,[51] P.Laurikainen,[23] M.Lebeau,[19] A.Lebedev,[17] P.Lebrun,[27] P.Lecomte,[51] P.Lecoq,[19] P.Le Coultre,[51] J.M.Le Goff,[19] R.Leiste,[50] E.Leonardi,[39] P.Levtchenko,[40] C.Li,[22] C.H.Lin,[53] W.T.Lin,[53] F.L.Linde,[2,19] L.Lista,[31] Z.A.Liu,[8] W.Lohmann,[50] E.Longo,[39] W.Lu,[35] Y.S.Lu,[8] K.Lübelsmeyer,[1] C.Luci,[39] D.Luckey,[17] L.Luminari,[39] W.Lustermann,[49] W.G.Ma,[22] M.Maity,[11] G.Majumder,[11] L.Malgeri,[39] A.Malinin,[30] C.Maña,[28] D.Mangeol,[33] S.Mangla,[11] P.Marchesini,[51] A.Marin,[12] J.P.Martin,[27] F.Marzano,[39] G.G.G.Massaro,[2] D.McNally,[19] R.R.McNeil,[7] S.Mele,[31] L.Merola,[31] M.Meschini,[18] W.J.Metzger,[33] M.von der Mey,[1] Y.Mi,[24] A.Mihul,[14] A.J.W.van Mil,[33] G.Mirabelli,[39] J.Mnich,[19] P.Molnar,[9] B.Monteleoni,[18] R.Moore,[3] S.Morganti,[39] T.Moulik,[11] R.Mount,[35] S.Müller,[1] F.Muheim,[21] A.J.M.Muijs,[2] S.Nahn,[17] M.Napolitano,[31] F.Nessi-Tedaldi,[51] H.Newman,[35] T.Niessen,[1] A.Nippe,[1] A.Nisati,[39] H.Nowak,[50] Y.D.Oh,[45] H.Opitz,[1] G.Organtini,[39] R.Ostonen,[23] C.Palomares,[28] D.Pandoulas,[1] S.Paoletti,[39] P.Paolucci,[31] H.K.Park,[37] I.H.Park,[45] G.Pascale,[39] G.Passaleva,[18] S.Patricelli,[31] T.Paul,[13] M.Pauluzzi,[36] C.Paus,[1] F.Pauss,[51] D.Peach,[19] Y.J.Pei,[1] S.Pensotti,[29] D.Perret-Gallix,[4] B.Petersen,[33] S.Petrak,[9] A.Pevsner,[5] D.Piccolo,[31] M.Pieri,[18] J.C.Pinto,[37] P.A.Piroué,[38] E.Pistolesi,[29] V.Plyaskin,[30] M.Pohl,[51] V.Pojidaev,[30,18] H.Postema,[17] N.Produit,[21] D.Prokofiev,[40] G.Rahal-Callot,[51] N.Raja,[11] P.G.Rancoita,[29] M.Rattaggi,[29] G.Raven,[42] P.Razis,[32] K.Read,[34] D.Ren,[51] M.Rescigno,[39] S.Reucroft,[13] T.van Rhee,[47] S.Riemann,[50] K.Riles,[3] A.Robohm,[51] J.Rodin,[17] B.P.Roe,[3] L.Romero,[28] S.Rosier-Lees,[4] Ph.Rosselet,[24] W.van Rossum,[47] S.Roth,[1] J.A.Rubio,[19] D.Ruschmeier,[9] H.Rykaczewski,[51] J.Salicio,[19] E.Sanchez,[28] M.P.Sanders,[33] M.E.Sarakinos,[23] S.Sarkar,[11] M.Sassowsky,[1] C.Schäfer,[1] V.Schegelsky,[40] S.Schmidt-Kaerst,[1] D.Schmitz,[1] P.Schmitz,[1] N.Scholz,[51] H.Schopper,[52] D.J.Schotanus,[33] J.Schwenke,[1] G.Schwering,[1] C.Sciacca,[31] D.Sciarrino,[21] L.Servoli,[36] S.Shevchenko,[35] N.Shivarov,[44] V.Shoutko,[30] J.Shukla,[26] E.Shumilov,[30] A.Shvorob,[35] T.Siedenburg,[1] D.Son,[45] A.Sopczak,[50] B.Smith,[17] P.Spillantini,[18] M.Steuer,[17] D.P.Stickland,[38] A.Stone,[7] H.Stone,[38] B.Stoyanov,[44] A.Straessner,[1] K.Strauch,[16] K.Sudhakar,[11] G.Sultanov,[20] L.Z.Sun,[22] G.F.Susinno,[21] H.Suter,[51] J.D.Swain,[20] X.W.Tang,[8] L.Tauscher,[6] L.Taylor,[13] Samuel C.C.Ting,[17] S.M.Ting,[17] M.Tonutti,[1] S.C.Tonwar,[11] J.Tóth,[15] C.Tully,[38] H.Tuchscherer,[46] K.L.Tung,[8] Y.Uchida,[17] J.Ulbricht,[51] U.Uwer,[19] E.Valente,[39] R.T.Van de Walle,[33] G.Vesztergombi,[15] I.Vetlitsky,[30] G.Viertel,[51] M.Vivargent,[4] R.Völkert,[50] H.Vogel,[37] H.Vogt,[50] I.Vorobiev,[30] A.A.Vorobyov,[40] A.Vorvolakos,[32] M.Wadhwa,[6] W.Wallraff,[1] J.C.Wang,[17] X.L.Wang,[22] Z.M.Wang,[22] A.Weber,[1] F.Wittgenstein,[19] S.X.Wu,[20] S.Wynhoff,[1] J.Xu,[12] Z.Z.Xu,[22] B.Z.Yang,[22] C.G.Yang,[8] X.Y.Yao,[8] J.B.Ye,[22] S.C.Yeh,[53] J.M.You,[37] An.Zalite,[40] Yu.Zalite,[40] P.Zemp,[51] Y.Zeng,[1] Z.Zhang,[8] Z.P.Zhang,[22] B.Zhou,[12] G.Y.Zhu,[8] R.Y.Zhu,[35] A.Zichichi,[10,19,20] F.Ziegler.[50]

1 I. Physikalisches Institut, RWTH, D-52056 Aachen, FRG[§]
III. Physikalisches Institut, RWTH, D-52056 Aachen, FRG[§]
2 National Institute for High Energy Physics, NIKHEF, and University of Amsterdam, NL-1009 DB Amsterdam, The Netherlands
3 University of Michigan, Ann Arbor, MI 48109, USA
4 Laboratoire d'Annecy-le-Vieux de Physique des Particules, LAPP,IN2P3-CNRS, BP 110, F-74941 Annecy-le-Vieux CEDEX, France
5 Johns Hopkins University, Baltimore, MD 21218, USA
6 Institute of Physics, University of Basel, CH-4056 Basel, Switzerland
7 Louisiana State University, Baton Rouge, LA 70803, USA
8 Institute of High Energy Physics, IHEP, 100039 Beijing, China[△]
9 Humboldt University, D-10099 Berlin, FRG[§]
10 University of Bologna and INFN-Sezione di Bologna, I-40126 Bologna, Italy
11 Tata Institute of Fundamental Research, Bombay 400 005, India
12 Boston University, Boston, MA 02215, USA
13 Northeastern University, Boston, MA 02115, USA
14 Institute of Atomic Physics and University of Bucharest, R-76900 Bucharest, Romania
15 Central Research Institute for Physics of the Hungarian Academy of Sciences, H-1525 Budapest 114, Hungary[‡]
16 Harvard University, Cambridge, MA 02139, USA
17 Massachusetts Institute of Technology, Cambridge, MA 02139, USA
18 INFN Sezione di Firenze and University of Florence, I-50125 Florence, Italy
19 European Laboratory for Particle Physics, CERN, CH-1211 Geneva 23, Switzerland
20 World Laboratory, FBLJA Project, CH-1211 Geneva 23, Switzerland
21 University of Geneva, CH-1211 Geneva 4, Switzerland
22 Chinese University of Science and Technology, USTC, Hefei, Anhui 230 029, China[△]
23 SEFT, Research Institute for High Energy Physics, P.O. Box 9, SF-00014 Helsinki, Finland
24 University of Lausanne, CH-1015 Lausanne, Switzerland
25 INFN-Sezione di Lecce and Universitá Degli Studi di Lecce, I-73100 Lecce, Italy
26 Los Alamos National Laboratory, Los Alamos, NM 87544, USA
27 Institut de Physique Nucléaire de Lyon, IN2P3-CNRS,Université Claude Bernard, F-69622 Villeurbanne, France
28 Centro de Investigaciones Energeticas, Medioambientales y Tecnologicas, CIEMAT, E-28040 Madrid, Spain[♭]
29 INFN-Sezione di Milano, I-20133 Milan, Italy
30 Institute of Theoretical and Experimental Physics, ITEP, Moscow, Russia
31 INFN-Sezione di Napoli and University of Naples, I-80125 Naples, Italy
32 Department of Natural Sciences, University of Cyprus, Nicosia, Cyprus
33 University of Nijmegen and NIKHEF, NL-6525 ED Nijmegen, The Netherlands
34 Oak Ridge National Laboratory, Oak Ridge, TN 37831, USA
35 California Institute of Technology, Pasadena, CA 91125, USA
36 INFN-Sezione di Perugia and Universitá Degli Studi di Perugia, I-06100 Perugia, Italy
37 Carnegie Mellon University, Pittsburgh, PA 15213, USA
38 Princeton University, Princeton, NJ 08544, USA
39 INFN-Sezione di Roma and University of Rome, "La Sapienza", I-00185 Rome, Italy
40 Nuclear Physics Institute, St. Petersburg, Russia
41 University and INFN, Salerno, I-84100 Salerno, Italy
42 University of California, San Diego, CA 92093, USA
43 Dept. de Fisica de Particulas Elementales, Univ. de Santiago, E-15706 Santiago de Compostela, Spain
44 Bulgarian Academy of Sciences, Central Lab. of Mechatronics and Instrumentation, BU-1113 Sofia, Bulgaria
45 Center for High Energy Physics, Korea Adv. Inst. of Sciences and Technology, 305-701 Taejon, Republic of Korea
46 University of Alabama, Tuscaloosa, AL 35486, USA
47 Utrecht University and NIKHEF, NL-3584 CB Utrecht, The Netherlands
48 Purdue University, West Lafayette, IN 47907, USA
49 Paul Scherrer Institut, PSI, CH-5232 Villigen, Switzerland
50 DESY-Institut für Hochenergiephysik, D-15738 Zeuthen, FRG
51 Eidgenössische Technische Hochschule, ETH Zürich, CH-8093 Zürich, Switzerland
52 University of Hamburg, D-22761 Hamburg, FRG
53 High Energy Physics Group, Taiwan, China

§ Supported by the German Bundesministerium für Bildung, Wissenschaft, Forschung und Technologie
‡ Supported by the Hungarian OTKA fund under contract numbers T14459 and T24011.
♭ Supported also by the Comisión Interministerial de Ciencia y Tecnología
♯ Also supported by CONICET and Universidad Nacional de La Plata, CC 67, 1900 La Plata, Argentina
♢ Also supported by Panjab University, Chandigarh-160014, India
△ Supported by the National Natural Science Foundation of China.

Selection of Process	Efficiencies [%] for $qqe\nu$	$qq\mu\nu$	$qq\tau\nu$	$\ell\nu\ell\nu$	$qqqq$	Background [pb]	Systematic Error [%]
$e^+e^- \to qqe\nu(\gamma)$	79.3	0.16	1.74			0.063	3
$e^+e^- \to qq\mu\nu(\gamma)$	0.11	74.1	3.50			0.037	3
$e^+e^- \to qq\tau\nu(\gamma)$	5.62	6.89	46.6		0.14	0.207	5
$e^+e^- \to \ell\nu\ell\nu(\gamma)$				45.1		0.033	4
$e^+e^- \to qqqq(\gamma)$	0.08	0.04	2.14		84.1	1.23	3

Table 1: Selection efficiencies, accepted background cross sections from non-W processes, and total systematic uncertainties for signal processes $e^+e^- \to qqe\nu(\gamma)$, $e^+e^- \to qq\mu\nu(\gamma)$, $e^+e^- \to qq\tau\nu(\gamma)$, $e^+e^- \to \ell\nu\ell\nu(\gamma)$ and $e^+e^- \to qqqq(\gamma)$. For the $qqe\nu$ ($\ell\nu\ell\nu$) signal, the signal efficiency is derived from a CC20 (CC56+NC56) Monte Carlo sample and is given within phase-space cuts, see Section 2.1 (2.4). For the $qqqq$ signal, the numbers are quoted for a neural-network output larger than 0.72. The total systematic uncertainties are relative to the cross sections listed in Table 2.

Process	$N_{\rm data}$	$N_{\rm bg}$	σ(cuts) [pb]	σ(CC03) [pb]	$r_{\rm SM}$ [%]	$\sigma_{\rm SM}$ [pb]
$e^+e^- \to qqe\nu(\gamma)$	19	0.64	$2.22^{+0.58}_{-0.50} \pm 0.07$	$2.44^{+0.64}_{-0.55} \pm 0.07$	14.6	1.81
$e^+e^- \to qq\mu\nu(\gamma)$	9	0.38	—	$1.06^{+0.44}_{-0.36} \pm 0.03$	14.6	1.81
$e^+e^- \to qq\tau\nu(\gamma)$	12	2.12	—	$1.60^{+0.81}_{-0.67} \pm 0.08$	14.6	1.81
$e^+e^- \to \ell\nu\ell\nu(\gamma)$	9	0.34	$1.87^{+0.72}_{-0.58} \pm 0.08$	$1.93^{+0.74}_{-0.60} \pm 0.08$	10.6	1.32
$e^+e^- \to qqqq(\gamma)$	61	12.6	—	$5.48^{+0.92}_{-0.85} \pm 0.17$	45.6	5.67

Table 2: Number of selected data events, $N_{\rm data}$, number of expected non-W background events, $N_{\rm bg}$, and cross sections for the reactions $e^+e^- \to qqe\nu(\gamma)$, $e^+e^- \to qq\mu\nu(\gamma)$, $e^+e^- \to qq\tau\nu(\gamma)$, $e^+e^- \to \ell\nu\ell\nu(\gamma)$ and $e^+e^- \to qqqq(\gamma)$. For the $qqqq$ signal, the numbers $N_{\rm data}$ and $N_{\rm bg}$ correspond to a cut on the output of the neural network at 0.72. The $qqqq$ cross section is obtained from a fit to the neural-network output distribution as described in Section 2.5. For the $qqe\nu$ and $\ell\nu\ell\nu$ signal, the cross sections within the phase-space cuts described in the text, σ(cuts), are given in addition to the CC03 cross sections, σ(CC03). The first error is statistical and the second systematic. Also shown are the CC03 ratios, $r_{\rm SM}$, and the CC03 cross sections, $\sigma_{\rm SM}$, as expected within the Standard Model.

Parameter	Lepton Non-Universality	Lepton Universality	Standard Model
$B(\mathrm{W} \to \mathrm{e}\nu)$ [%]	$16.5^{+3.7}_{-3.3} \pm 0.5$	—	
$B(\mathrm{W} \to \mu\nu)$ [%]	$8.4^{+2.8}_{-2.4} \pm 0.3$	—	
$B(\mathrm{W} \to \tau\nu)$ [%]	$10.9^{+4.2}_{-3.9} \pm 0.5$	—	
$B(\mathrm{W} \to \ell\nu)$ [%]	—	$11.9^{+1.3}_{-1.2} \pm 0.2$	10.8
$B(\mathrm{W} \to qq)$ [%]	$64.2^{+3.7}_{-3.8} \pm 0.5$	$64.2^{+3.7}_{-3.8} \pm 0.5$	67.5
σ_{WW} [pb]	$12.37^{+1.47}_{-1.37} \pm 0.23$	$12.40^{+1.44}_{-1.34} \pm 0.23$	12.43

Parameter	Using SM W-Decay Branching Fractions	Standard Model
σ_{WW} [pb]	$12.27^{+1.41}_{-1.32} \pm 0.23$	12.43

Table 3: W-decay branching fractions, B, and total W-pair cross section, σ_{WW}, derived with and without the assumption of charged-current lepton universality. In the bottom part of the table, the measured total W-pair cross section imposing Standard-Model W-decay branching fractions is given. Also shown are the W-decay branching fractions [5] and the total W-pair cross section as expected in the Standard Model.

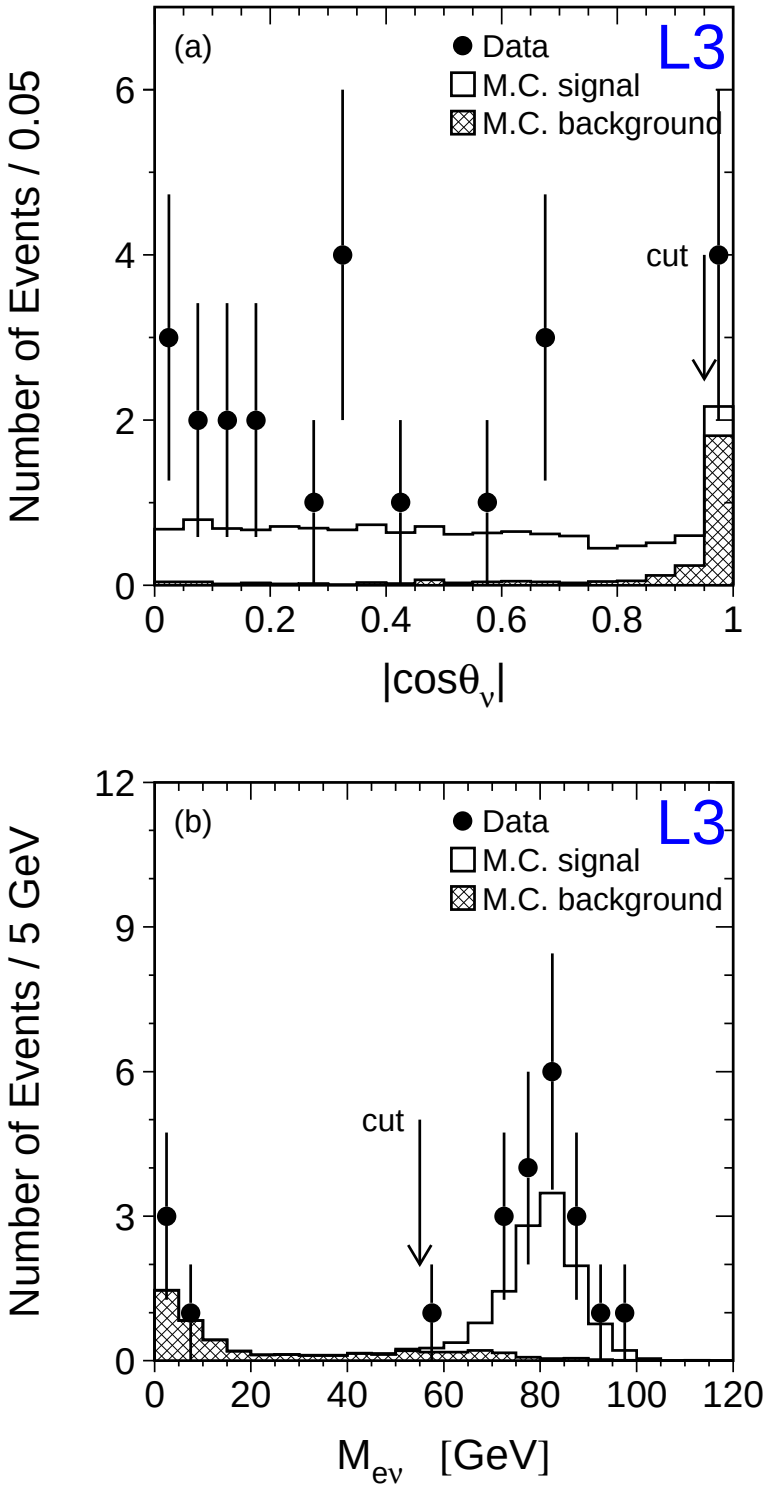

Figure 1: Distributions of variables used for the selection of $e^+e^- \to qqe\nu(\gamma)$ events, comparing the signal and background Monte Carlo to the data. The position of the selection cuts are indicated by vertical arrows. All selection cuts except in the variable plotted are applied. (a) The polar angle of the neutrino, $|\cos\theta_\nu|$. (b) The invariant mass of the electron-neutrino system, $M_{e\nu}$.

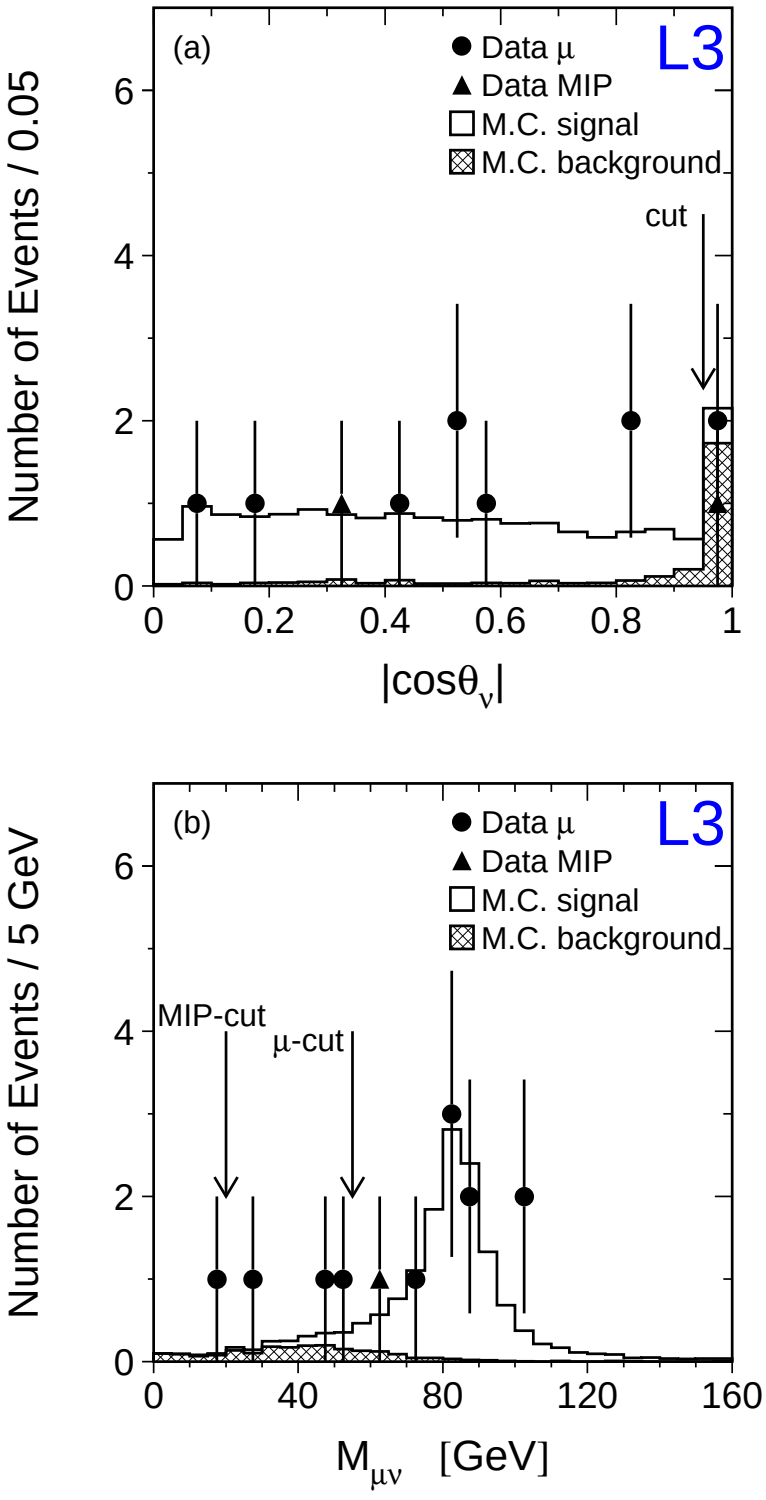

Figure 2: Distributions of variables used for the selection of $e^+e^- \to qq\mu\nu(\gamma)$ events. (a) The polar angle of the neutrino, $|\cos\theta_\nu|$. (b) The invariant mass of the muon-neutrino system, $M_{\mu\nu}$.

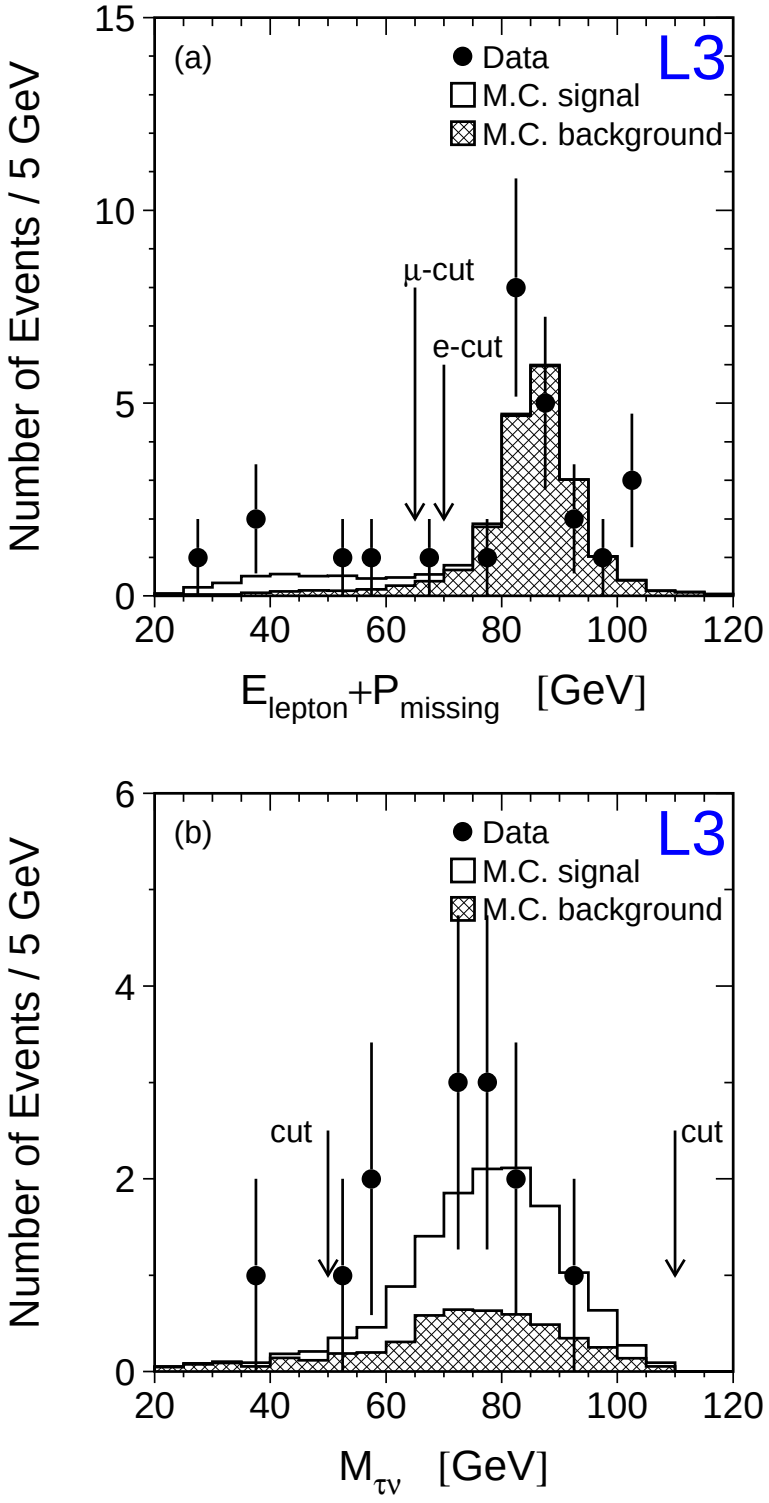

Figure 3: Distributions of variables used for the selection of $e^+e^- \to qq\tau\nu(\gamma)$ events. (a) The sum of the electron (muon) energy and the missing momentum, $E_{\rm lepton} + P_{\rm missing}$, used in the selection for leptonic τ decays. (b) The invariant mass of the system of the τ jet and the missing four-momentum, $M_{\tau\nu}$.

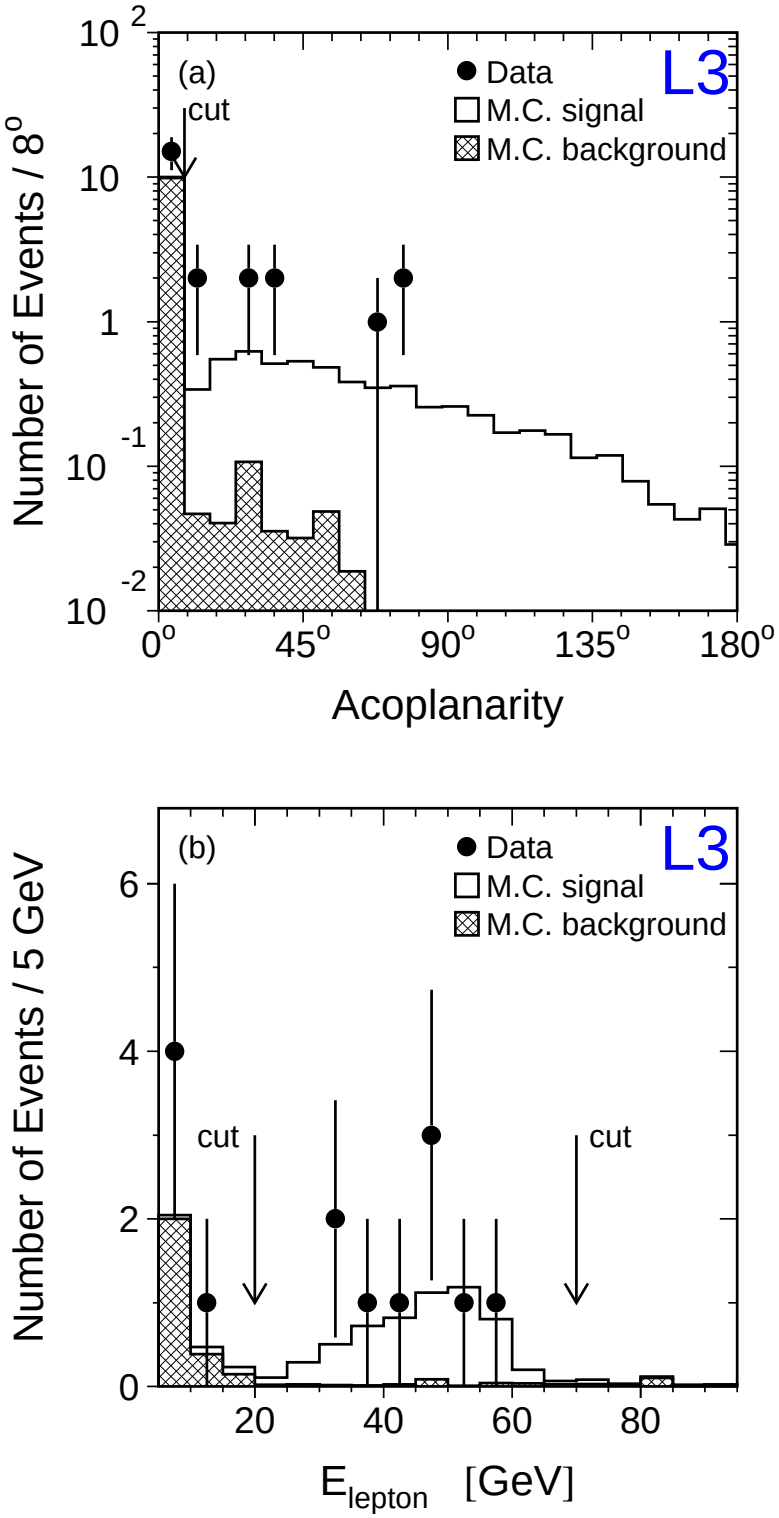

Figure 4: Distributions of variables used for the selection of $e^+e^- \to \ell\nu\ell\nu(\gamma)$ events. (a) The acoplanarity between the two charged leptons. (b) The energy of the identified electron or muon with highest energy, $E_{\rm lepton}$.

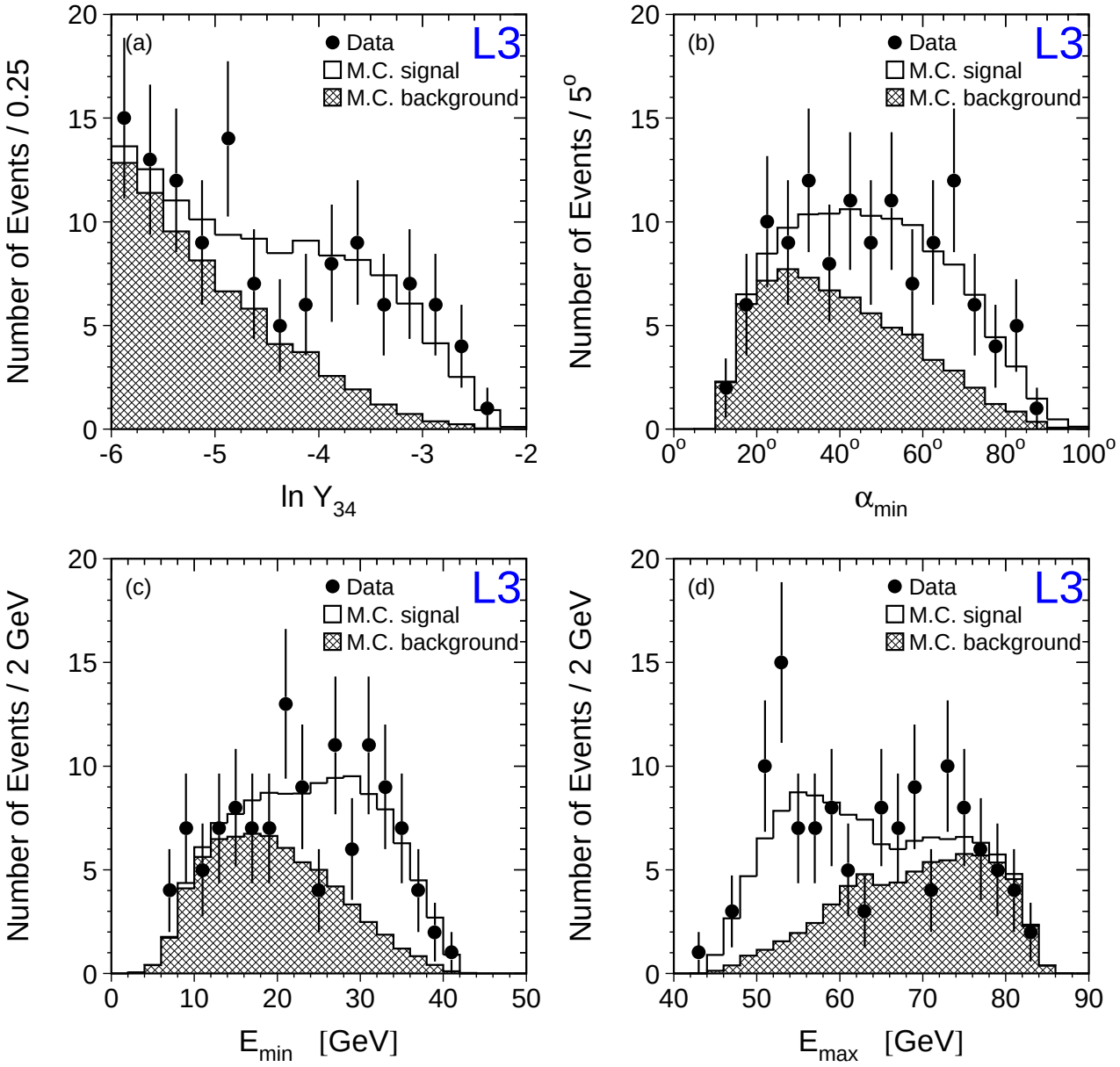

Figure 5: Distributions of variables used for the neural network in the analysis of $e^+e^- \to qqqq(\gamma)$ events. All selection cuts are applied. (a) The jet resolution parameter, Y_{34}. (b) The minimal jet-jet angle, $\alpha_{\rm min}$. (c) The minimal jet energy, $E_{\rm min}$. (d) The maximal jet energy, $E_{\rm max}$.

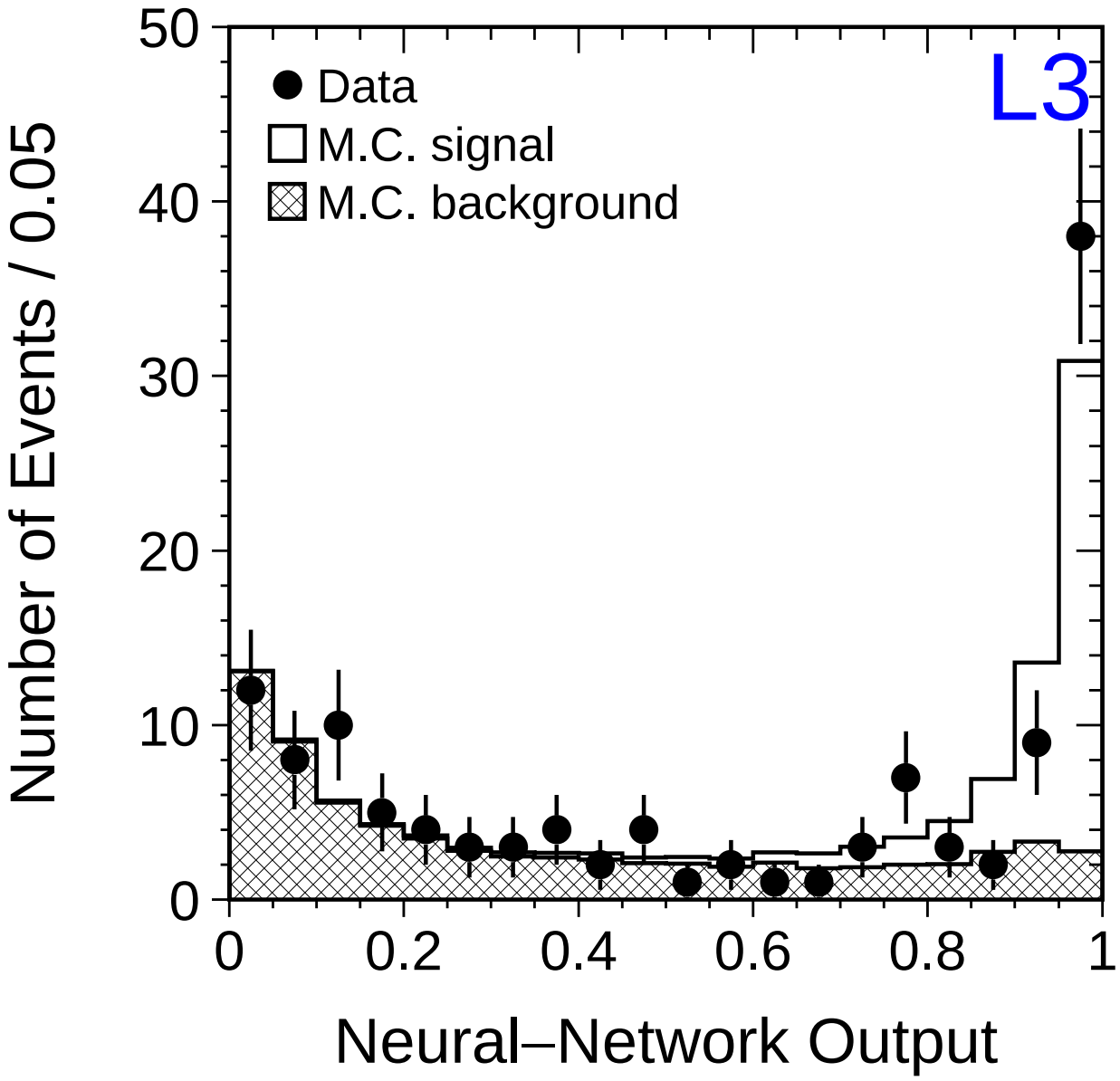

Figure 6: Distribution of the output of the neural network used in the analysis of $e^+e^- \to qqqq(\gamma)$ events.

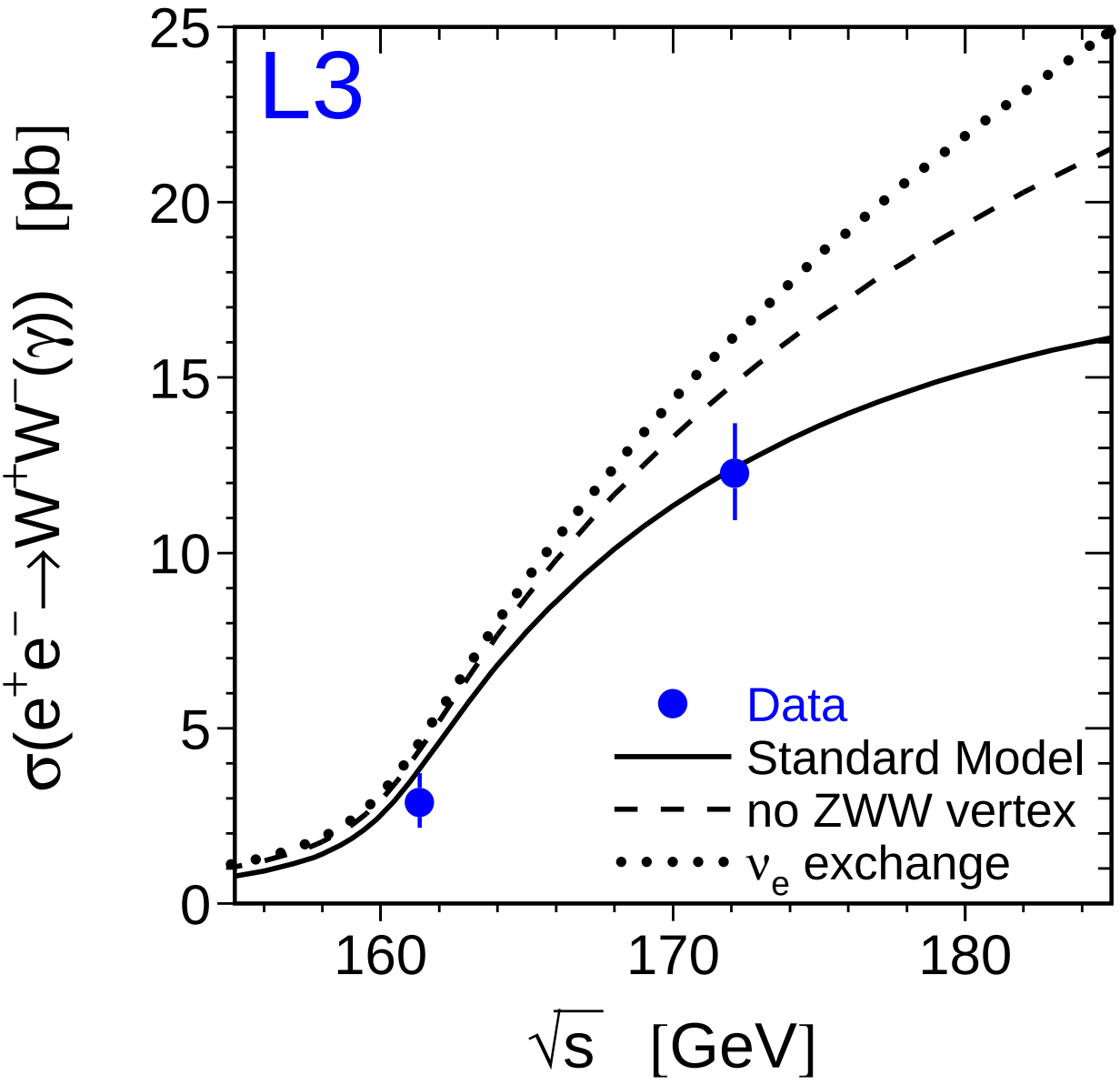

Figure 7: The cross section, σ_{WW}, of the process $\mathrm{e^+e^-} \to \mathrm{WW} \to ffff(\gamma)$ as a function of the centre-of-mass energy, $\sqrt{s}$. The measurements of σ_{WW} at $\sqrt{s} = 161$ GeV [1] and at $\sqrt{s} = 172$ GeV are shown as dots with error bars, combining statistical and systematic errors in quadrature. The solid curve shows the Standard Model expectation. The dashed curve shows the expectation if there is no ZWW coupling. The dotted curve shows the expectation if only t-channel ν_{e} exchange in W-pair production is considered.